2012 12th International Conference on Control, Automation, Robotics & Vision
Guangzhou, China, 5-7th December 2012 (ICARCV 2012)

A Simple Robust Controller for Hysteresis and Resonance Compensation of Piezoelectric Actuators

Jinchuan Zheng
Faculty of Engineering and Industrial Sciences
Swinburne University of Technology
Hawthorn, VIC 3128, Australia
Email: jzheng@swin.edu.au

Minyue Fu
School of Electrical Engineering and Computer Science
The University of Newcastle
Callaghan, NSW 2308, Australia
Email: minyue.fu@newcastle.edu.au

***Abstract*—Hysteresis and resonance dynamics are typical adverse effects associated with the piezoelectric (PZT) actuators. To eliminate the loss of positioning accuracy due to these effects, we propose a simple two degree-of-freedom (2DOF) control scheme for the PZT actuators, which consists of a feedforward and a feedback compensator for hysteresis and resonance compensation and for robust step reference tracking. Despite the proposed controller is on par with the existing 2DOF control methods, its specific structure offers significant design simplicity. The experimental results on an actual PZT nanopositioner show that the designed controller can be easily implemented and achieve superior performance for hysteresis and resonance compensation.**

I. Introduction

The piezoelectric (PZT) actuator is a well-known device for precision positioning and motion control. It is fabricated using piezoelectric materials which have the property of converting electrical energy to mechanical energy. By applying an electric potential to the piezoelectric material, the PZT actuator can produce extremely small displacements in the range of subnanometer to a few hundreds micrometers. PZT actuators have been widely used in a variety of applications such as optical trapping [1], biotechnology [2], high precision dual-stage actuation [3]–[5], and nanomanipulation [6]. Particularly, in atomic force microscope (AFM) [7], [8] and scanning probe microscopy (SPM) [9] nowadays, PZT actuators have been an indispensable component to displace the sensor probe over a sample surface to collect the surface property information at the nanometer resolution. Moreover, the PZT actuated nanopositioning systems [10], [11] are also needed in semiconductor test equipment for the positioning of wafers and mask alignments.

When feedback control and an accurate PZT model for feedforward control are unavailable, the PZT actuator can only be used for applications that require moderate precision. The resulting displacement roughly corresponds to the drive voltage. However, for long-range operations the positioning precision can be significantly degraded due to the nonlinear hysteresis and creep effects that are common properties with PZT actuators. It has been reported that hysteresis effect can be reduced by the use of charge or current sources to drive the PZT actuators (see e.g., [12], [13]). However, the main difficulty is the existence of offset voltages in the charge or current source circuit and the uncontrolled nature of the output voltage, which results in the capacitive load being charged up [14]. Alternatively, the use of voltage amplifier combined with servo control is a popular approach for its easy implementation and its capability of virtual elimination of the hysteresis and creep effects. Furthermore, a well-designed controller can provide extra benefits such as vibration compensation and maintaining robustness. In this paper, we also use a voltage power amplifier and aim to design an effective controller for the PZT actuator to compensate for the hysteresis and vibrations and to achieve fast tracking response.

A thorough literature review on control approaches for PZT actuators is reported in [14] and [15]. In particular, for hysteresis and vibration compensations there are three main approaches: inversion-based feedforward [16], high-gain feedback [17], and combined feedforward-feedback control [18]. In the inversion-based feedforward approach, an accurate hysteresis and vibrational dynamic model is crucial for the effectiveness of the compensation because the desired output is fed through the inverse model to generate feedforward signals to cancel the hysteresis and vibrations. For this reason, a variety of hysteresis models are reported (see e.g., [19]–[21]) to capture the static and even the dynamic (rate-dependent) hysteresis behavior. However, such feedforward-based methods are essentially open-loop control systems and thus the performance is sensitive to modeling error. Moreover, inversion of the high-order hysteresis nonlinear model generally results in computational complexity [14]. On the contrary, the high-gain feedback approach avoids the need for an accurate model. In such methods [22], [23], hysteresis and vibrations are essentially regarded as input disturbances and the induced position error is detected by the position sensor and fed back to the controller to generate PZT control signals to correct for position errors. Generally, the high-gain feedback control provides an effective and more robust method to suppress the hysteresis and vibrations and thus, is commonly used for positioning tasks which require high precision, repeatability, and long-term stability. To obtain the advantages of both feedforward and feedback control, a combined feedforward-feedback control approach has also been proposed, where the high-gain feedback control is used to linearize the nonlinear hysteresis and creep, and a feedforward input is found to ac-

978-1-4673-1872-3/12/$31.00 ©2012 IEEE

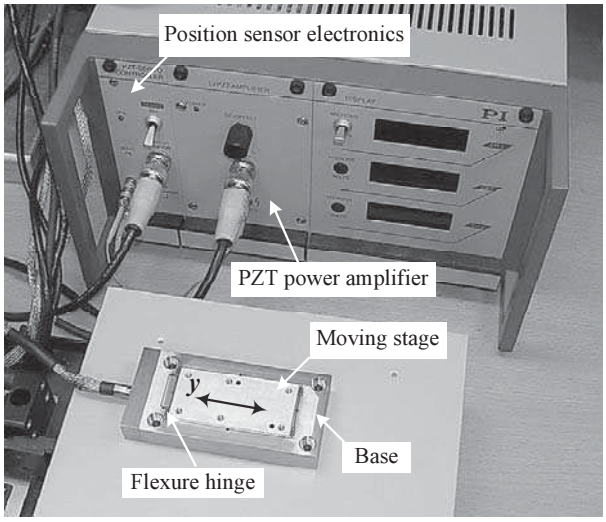

Fig. 1. Experimental setup of the PZT actuated nanopositioner (The PZT actuator and position sensor are attached to the moving stage and embedded into the base).

count vibration [18], [24]. This design method is demonstrated to achieve high-precision high-speed positioning with robust performance and easy implementation.

In this paper, we develop a controller which combines the feedforward inversion and high-gain feedback control structure to cope with the hysteresis and resonance vibrations. We note that our controller is essentially another form of two degree-of-freedom (2DOF) control structures. However, our controller is parameterized by a unique Q-filter which characterizes the closed-loop transfer function. This provides advantages in design simplicity and easy implementation. This paper is organized as follows. Section II introduces the experimental setup and plant modeling of the PZT actuator nanopositioning system. Section III develops the controller for hysteresis and resonance compensation. Robust analysis of the closed-loop system is also given. Section IV shows the experimental results to demonstrate the effectiveness of the proposed design. Section V concludes the paper.

II. Plant Modeling

Fig. 1 shows the experimental setup of the PZT actuated nanopositioner (P-752, Polytec PI) studied in this paper. The nanopositioner comprises a flexure-guided moving stage that is driven by a PZT microactuator with a travel range of ± 12.5 μm, and a capacitive position sensor with a practical resolution of 14 nm to measure the displacement of the moving stage along the axis. The position sensor output is fedback to a real-time DSP system (dSPACE-DS1103) on which the feedback controller is implemented with the sampling frequency of 20 kHz. Subsequently, the control signal is passed through the power amplifier to output control voltage for the PZT actuator.

To clarify the associated dynamics and gains of the system, a block diagram is presented in Fig. 2. The power amplifier used is essentially a voltage amplifier that has a static gain of 10 V/V. The control input to the power amplifier denoted by u_p

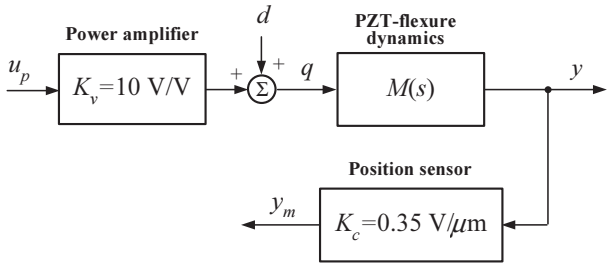

Fig. 2. Block diagram of the PZT actuated nanopositioner plant model, where u_p is the applied voltage input, d indicates the input disturbances including the hysteresis effects, q is the charge between the PZT electrodes, y is the actual displacement of the PZT positioner, and y_m is the capacitive position sensor output.

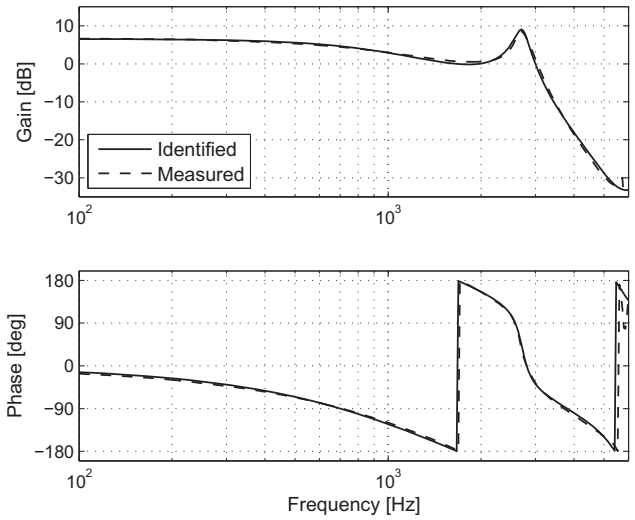

Fig. 3. Frequency responses of the PZT nanopositioner model $P(s)$.

is limited to have an amplitude within ± 4.4 V corresponding to the travel range of the PZT actuator. The capacitive position sensor has a static gain of 0.35 V/μm. The nonlinear hysteresis effect of the PZT is modeled as a bounded input disturbance d [17] between the applied actuator-voltage and the PZT-flexure dynamic model. Although a mathematical model of the hysteresis can be obtained through experimental data [21], it is considered trivial for the control design in our study since a feedback control scheme will be used for hysteresis compensation rather than model inversion-based approaches such as [16]. The PZT-flexure dynamics include the PZT electromechanical model [25] and the flexure vibration model. More specifically, it can be expressed as a sum of a number of resonance modes as follows

$$M(s) = \sum_{i=1}^{N} \frac{B_i s + A_i}{s^2 + 2\zeta_i \omega_i s + \omega_i^2} + D, \qquad (1)$$

where D is a feed-through term related to the zero locations of the system and it is found useful to better match the high-frequency roll-off characteristics. N is the total number of resonance modes that sufficiently describe the structure properties in the frequency of interest. ζ_i, ω_i and A_i are the

TABLE I
MODAL PARAMETERS OF $M(s)$

Mode (i)	ω_i	ζ_i	A_i	B_i
1	$2\pi 1018$	0.883	9.138×10^6	-736.62
2	$2\pi 2721$	0.051	-4.623×10^6	459.0
$D = 5.140 \times 10^{-3}$				

damping ratio, the resonance frequency and the modal constant of mode i, respectively. B_i is the resonance coupling parameter of mode i, which is used to match the non-minimum phase (NMP) characteristics.

The plant modal parameters are identified from experimental frequency response data. A dynamic signal analyzer (HP 35670A) is used to generate the swept-sinusoidal excitation signals and collect the frequency response data from the PZT control input signal u_p to the displacement output y that is scaled from the sensor output y_m. Hence, we can obtain the measured frequency response data for the plant model $P(s)$ expressed by

$$P(s) = \frac{y}{u_p} = K_v M(s). \tag{2}$$

The dashed lines in Fig. 3 show the measured frequency responses of $P(s)$ in the frequency range of interest. We can see that the system dynamics are dominated by two resonance modes whose resonance frequencies are 1018 and 2721 Hz, respectively. The first mode denotes the PZT electromechanical effect, whose resonance frequency typically decreases with a larger PZT capacitive load. Interested readers can refer to [25] for a detailed parameter electromechanical model. The second mode, caused by the flexibility of the flexure hinge, has a relatively large resonance peak (10 dB) and is thus expected to induce significant vibrations to the stage motion. From the point of view of control design, the first mode is generally the principal mode that limits the servo bandwidth; and the second mode should be actively damped for fast and smooth settling performance. Note that from the phase plot in Fig. 3, we also observe that the phase angle exhibits extra lag (e.g., within $3-5$ kHz) in addition to the phase lag associated with the resonance modes. This implies that the plant has strong non-minimum phase (NMP) antiresonance modes (i.e., NMP zeroes) within the frequency range.

The modal parameters in (1) can be identified from the measured frequency responses data by using the least square estimation method [26]. Table I lists the modal parameters obtained for $M(s)$. The solid lines in Fig. 3 indicate that the identified model has a close match with the measured model. In particular, the NMP characteristics of the plant is well captured by the identified model. Table II lists the poles and zeros pairs of the plant model $P(s)$ from which we can see that the plant model contains two pairs of complex NMP zeros whose resonance frequencies are located at 3151 and 5660 Hz, respectively. It should be emphasized that these NMP zeros will substantially degrade the achievable control bandwidth as will be clarified from the control analysis in the next section.

TABLE II
POLES AND ZEROS OF PLANT MODEL $P(s)$

Poles ($\times 10^4$)	Zeros ($\times 10^4$)
$-0.5645 \pm 0.2997j$	$1.4834 \pm 1.3092j$
$-0.0865 \pm 1.7063j$	$0.5690 \pm 3.5087j$

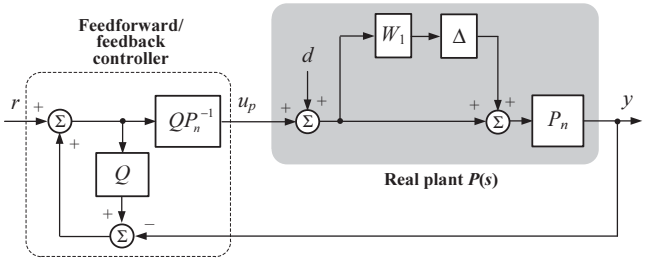

Fig. 4. Block diagram of combined feedforward/feedback control system for hysteresis and resonance compensation.

III. HYSTERESIS AND RESONANCE COMPENSATION

In this section, we study a combined feedforward/feedback control structure for hysteresis and resonance compensation to achieve the goal of fast and robust step tracking for the PZT nanopositioner.

A. Control Structure

Fig. 4 shows the block diagram of the combined feedforward/feedback control structure [27], where Q is the filter to be designed and we rewrite the real plant model $P(s)$ as

$$P = P_n(1 + W_1\Delta). \tag{3}$$

In the above, the nominal plant P_n represents the stable and minimum phase part of P and should satisfy

$$P_n \approx P \tag{4}$$

in low frequencies within 0-200 Hz. $\|\Delta\|_\infty < 1$ denotes a stable unstructured disk-like uncertainty; and W_1 represents a proper stable weighting function. The NMP behavior of the plant is treated as model uncertainty and described by W_1. Moreover, the magnitude of W_1 increases due to changes in the operating conditions such as PZT offset, reference input, and load variations. The model of W_1 due to these uncertainties can be experimentally measured. More specifically, we collect 10 frequency responses data of $P_i(j\omega_k)$, $i = 1 \ldots 10; k = 1 \ldots 800$. Each measurement is carried out under a different operation condition. The frequency responses of the perturbed plants are show in Fig. 5a. Then, the magnitude of W_1 can be derived by

$$|W_1(j\omega_k)| = \max_{i=1\ldots10} \left(\frac{|P_i(j\omega_k) - P_n(j\omega_k)|}{|P_n(j\omega_k)|} \right), \tag{5}$$

which is plotted in Fig. 5b. We can see that W_1 increases with frequency due to the relative uncertainty to the nominal plant model.

The control structure as shown in Fig. 4 is essentially a 2DOF control structure with a unique design parameter Q. It

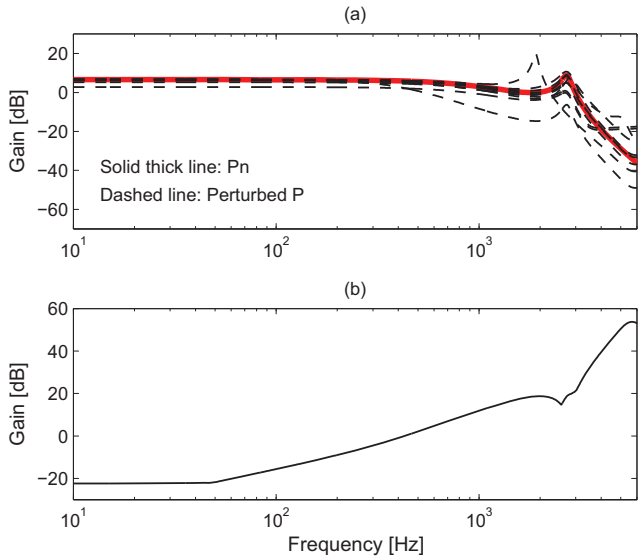

Fig. 5. (a) Frequency response of nominal plant model P_n (solid thick line) and perturbed plant models (dashed lines). (b) Magnitude of the relative uncertainty W_1 used for design and analysis.

unifies high-gain feedback idea (through Q) and the feedforward inversion principle (through P_n^{-1}) to yield a closed-loop dynamics as specified by Q. To see this, the transfer functions from respectively, the reference r and the disturbance d to the position output y can be easily obtained as follows

$$T_{yr} = \frac{QPP_n^{-1}}{1-Q(1-PP_n^{-1})}, \quad (6)$$

$$T_{yd} = \frac{(1-Q)P}{1-Q(1-PP_n^{-1})}. \quad (7)$$

According to (3), P_n can be obtained by removing the NMP zeros of P. We find that the resultant P_n satisfies (4) within 0–200 Hz. Note that the mismatch part is treated as plant uncertainty and will be compensated by the high-gain feedback control. Then, we summarize the design conditions of Q filter to meet our desired performance:

i) $\|W_1Q\|_\infty < 1$;

ii) Q filter is with low-pass characteristics and specifically has

$$Q(j\omega) \approx 1, \quad \forall \omega \in [0,\ \omega_b], \quad (8)$$

where ω_b denotes the frequency bandwidth of Q;

iii) $Q(j\omega_i) < -30$ dB, where ω_i $(i = 1, 2)$ equals the PZT resonance frequencies as listed in Table I;

iv) $\Upsilon(Q) \geq \Upsilon(P_n)$, where Υ denotes the relative degree (excess of poles over zeros).

The following remarks are given with regard to the design conditions above:

1) Condition i) is compulsory to guarantee the robust stability of the closed-loop system in Fig. 4. This can be seen by transforming Fig. 4 equivalent to Fig. 6, where $\tilde{r} = P_n^{-1}r$, $\tilde{d} = (1-Q)W_1d$. Now, according to the well-known small gain theorem [28], the interconnected system as shown in Fig. 6 is stable for all stable Δ with $\|\Delta\|_\infty \leq 1$ if and only if $\|W_1Q\|_\infty < 1$ holds.

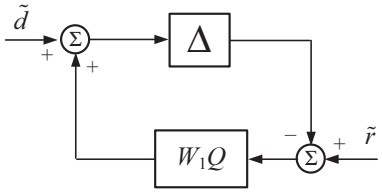

Fig. 6. Equivalent block diagram of Fig. 4 for robust stability analysis.

2) Substituting (4) and (8) into (6)–(7), respectively yields

$$T_{yr} \approx Q, \quad (9)$$

$$T_{yd} \approx 0 \quad (10)$$

for any $\omega \in [0,\ \omega_b]$. Now it is clear that the closed-loop dynamics can be easily specified by Q and is capable of rejecting those disturbances at low frequency range such as hysteresis. However, note that the maximum ω_b obtainable is generally subject to other conditions and particularly the sensing noise in practice.

3) Provided conditions i) and ii) hold, the ratio of resonance compensation is specified by condition iii). Typically, a larger ratio of resonance compensation is at the expense of reduced frequency bandwidth of $Q(s)$. Due to this, the frequency bandwidth of $Q(s)$ has be to selected substantially lower than the first resonance frequency.

4) Condition iv) is posed to ensure the controller QP_n^{-1} proper at least for practical implementation.

B. Controller Design

From the analysis above, the controller design is simply reduced to the design of the Q filter only, which in our particular application is chosen as

$$Q = \frac{1}{(\tau_0 s+1)^2(\tau_1 s+1)^3}, \quad (11)$$

where $\tau_0 = 8.0\times10^{-4}$ and $\tau_1 = 3.2\times10^{-5}$. For more details of general low-pass filters design, interested readers can refer to [29] and the references therein.

To verify the validity of the designed Q filter, Fig. 7 plots the magnitude of Q and W_1^{-1}, which indicates that the magnitudes of Q all lie below that of W_1^{-1} implying $\|W_1Q\|_\infty < 1$. In general, the magnitude of W_1^{-1} rolls off at high frequencies due to the plant uncertainty, thus constraining the achievable frequency bandwidth of Q filter. It is also straightforward to verify the satisfaction of the other design conditions in ii)-iv).

IV. Experimental Results

The designed controller is implemented on the actual PZT nanopositioner to demonstrate the performance of the control system for hysteresis and vibration compensation. First, we set the reference input r as sinusoidal signal with the amplitude sufficiently large to drive the PZT actuator to approach to its maximum range. Moreover, the sinusoidal frequency is chosen

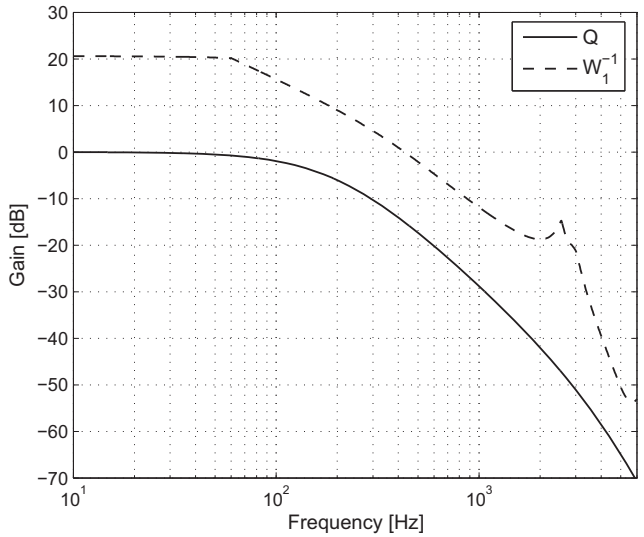

Fig. 7. Magnitude plots of Q filter and W_1^{-1}. The robust stability condition $\|W_1 Q\|_\infty < 1$ is equivalent to $Q(j\omega)$ curve being below $W_1(j\omega)^{-1}$ curve.

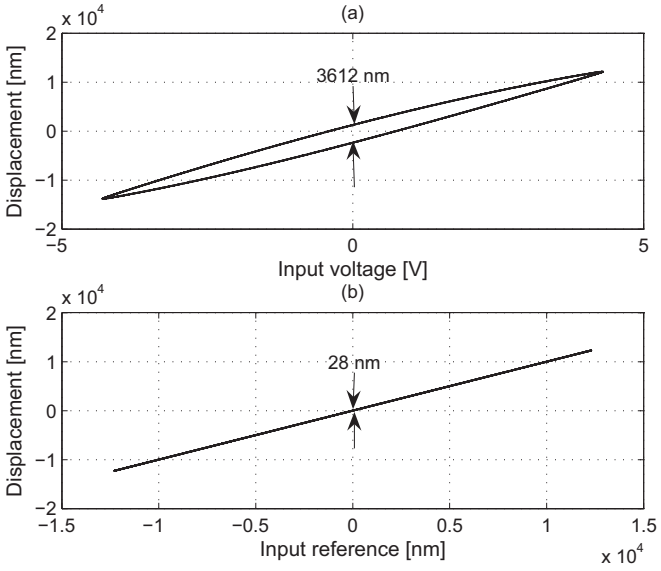

Fig. 8. Experimental results of hysteresis compensation. (a) Open-loop control; (b) 2DOF control. The maximum gap between the hysteresis loop is significantly reduced from 3612 nm to 28 nm when the 2DOF controller is applied.

sufficiently low (e.g. 0.1 Hz), at which the phase lag associated with the control loop is insignificant such that the input-output measurement reflects only the PZT hysteresis effect. This setting excites the worst hysteresis effects for a given input frequency and therefore is regarded as an effective approach to evaluate the designed controller. Fig. 8 shows the experimental results of the relationship between the PZT displacement and the reference input. We can see that with open-loop control the maximum gap between the hysteresis loop is 3612 nm (see Fig. 8a) and it is significantly reduced to 28 nm with the 2DOF controller (see Fig. 8b).

Next, Fig. 9 shows the measured frequency response of the

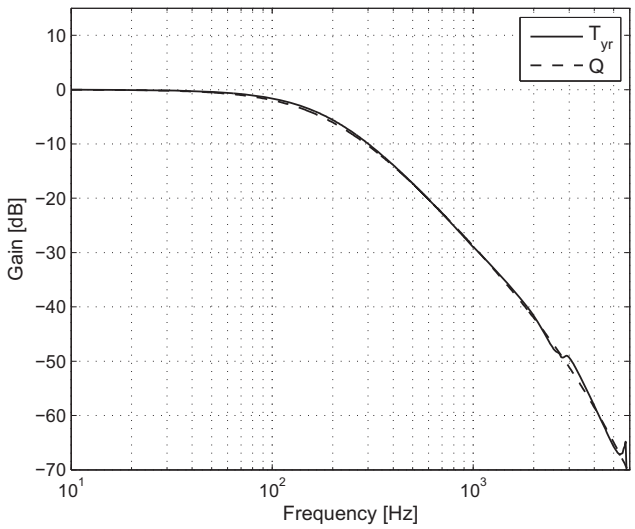

Fig. 9. Measured frequency responses of the closed-loop system. The magnitude of the resonant peak at 2.7 kHz is greatly damped, which is consistent with the design.

closed-loop system T_{yr} in comparison with its approximation Q. We can see that the resonance peaks at 1018 and 2721 Hz are highly damped by more than 30 dB. Furthermore, the experimental results of step tracking are shown in Fig. 10. We can clearly see that with open-loop control, the output displacement exhibits significant oscillations due to the resonant vibrations. With the 2DOF controller, the oscillations are almost removed from the output displacement. However, this benefit has to compromise with the relatively slow transient response because the closed-loop bandwidth has to be reduced to tolerate such uncertainties as hysteresis, NMP zeros and resonance modes.

Finally, we show a series of repeated step responses in Fig. 11, which indicates that the dynamic step responses are almost the same at various initial conditions. This verifies the robust performance of the controller against the hysteresis and resonant vibrations across the PZT work range.

V. Conclusion

We have developed a simple design method for hysteresis and resonance compensation. The designed controller is parameterized by a unique Q-filter based on which the robust stability condition is easily checked on the Bode plot (see Fig. 7) and the closed-loop dynamics is easily specified [see (9)]. The experimental results demonstrate that the control scheme can offer sufficient capability of hysteresis and resonance compensation and accurate step tracking control robustly.

References

[1] C. Mio, T. Gong, A. Terray, and D. Marr, "Design of a scanning laser optical trap for multiparticle manipulation," *Rev. Sci. Instrum.*, vol. 71, no. 5, pp. 2196-2200, May 2000.

[2] Q. Zou, K. Leang, E. Sadoun, M. Reed, and S. Devasia, "Control issues in high-speed AFM for biological applications: Collagen imaging example," *Asian J. Control: Special Issue Adv. Nano-Technol. Control,* vol. 6, no. 2, pp. 164-178, Jun. 2004.

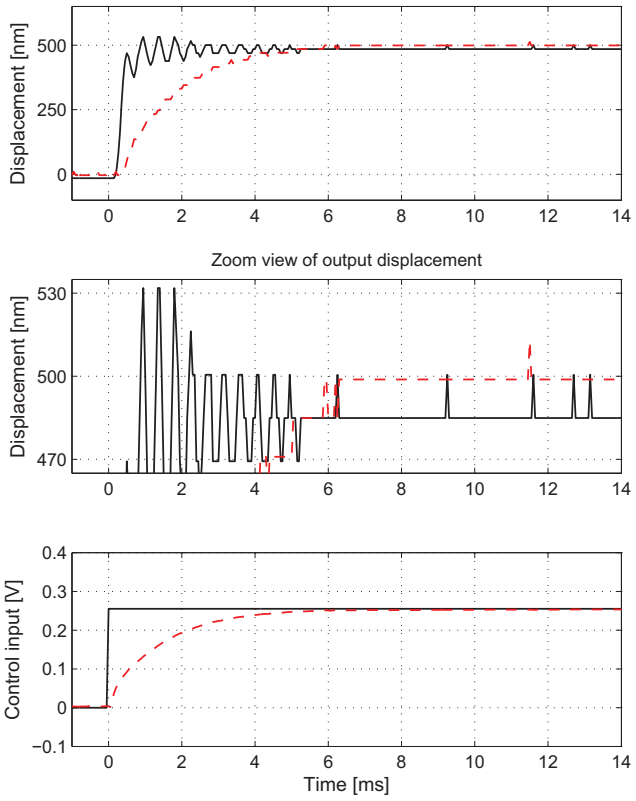

Fig. 10. Experimental results of step tracking responses. The oscillations are almost removed with the 2DOF controller. (Solid lines: open-loop control; dashed lines: with 2DOF controller)

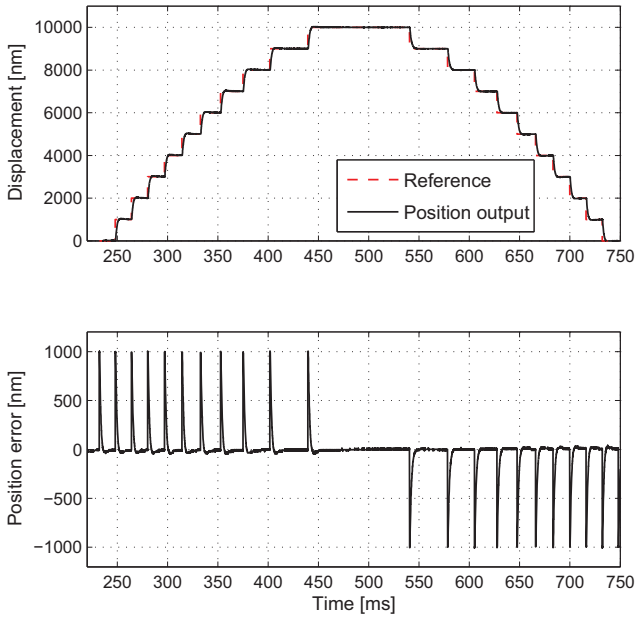

Fig. 11. Experimental results of repeated step responses from various initial conditions. The position error dynamic are almost the same in response to each step reference, which indicates the robust performance of the 2DOF controller against the hysteresis and resonant vibrations across the PZT work range.

[3] J. Zheng, W. Su, and M. Fu, "Dual-stage actuator control design using a doubly coprime factorization approach," *IEEE/ASME Trans. Mechatron.*, vol. 15, no. 3, pp. 339-348, Jun. 2010.

[4] J. Zheng, M. Fu, Y. Wang, and C. Du, "Nonlinear tracking control for a hard disk drive dual-stage actuator system," *IEEE/ASME Trans. Mechatron.*, vol. 13, no. 5, pp. 510-518, Oct. 2008.

[5] J. Zheng, A. Salton, and M. Fu, "Design and control of a rotary dual-stage actuator positioning system," *Mechatronics*, vol. 21, no. 6, pp. 1003-1012, Sep. 2011.

[6] H. Liaw, B. Shirinzadeh, and J. Smith, "Robust motion tracking control of piezo-driven flexure-based four-bar mechanism for micro/nano manipulation," *Mechatronics*, vol. 18, pp. 111-120, 2008.

[7] G. Binnig, C. Quate, and C. Gerber, "Atomic force microscope," *Phys. Rev. Lett.*, vol. 56, no. 9, pp. 930-933, Mar. 1986.

[8] N. Jalili and K. Laxminarayana, "A review of atomic force microscopy imaging systems: Application to molecular metrology and biological sciences," *Mechatronics*, vol. 14, no. 8, pp. 907-945, Oct. 2004.

[9] M. Yves, *Scanning Probe Microscopes*, Bellingham, WA: SPIE, 1995.

[10] H. Shakir and W. Kim "Nanoscale path planning and motion control for maglev nanopositioners," *IEEE/ASME Trans. Mechatron.*, vol. 11, no. 5, pp. 625-633, Oct. 2006

[11] J. Zheng, Y. Guo, M. Fu, Y. Wang, and L. Xie, "Development of an extended reset controller and its experimental demonstration," *IET Control Theory and Applications*, vol. 2, no. 10, pp. 866-874, 2008.

[12] A. Fleming and R. Moheimani, "Precision current and charge amplifiers for driving highly capacitive piezoelectric loads, *Electron. Lett.*, vol. 39, no. 3, pp. 282-284, Feb. 2003.

[13] R. Moheimani and B. Vautier, "Resonant control of structural vibration using charge-driven piezoelectric actuators," *IEEE Trans. Control Syst. Technol.*, vol. 13, no. 6, pp. 1021-1035, Nov. 2005.

[14] S. Devasia, E. Eleftheriou, and R. Moheimani, "A survey of control issues in nanopositioning," *IEEE Trans. Control Syst. Technol.*, vol. 15, no. 5, pp. 802-823, Sep. 2007.

[15] G. Clayton, S. Tien, K. Leang, Q. Zou, and S. Devasia, "A review of feedforward control approaches in nanopositioning for high-speed SPM," *J. Dyn. Syst., Meas. Control*, vol. 131, pp. 061101-1-19, Nov. 2009.

[16] D. Croft, G. Shed, and S. Devasia, "Creep, hysteresis, and vibration compensation for piezoactuators: atomic force microscopy application," *J. Dyn. Syst., Meas. Control*, vol. 123, pp. 35-43, Mar. 2001.

[17] J. Yi, S. Chang, and T. Shen, "Disturbance-observer-based hysteresis compensation for piezoelectric actuators," *IEEE/ASME Trans. Mechatron.*, vol. 14, no. 4, pp. 456-464, Aug. 2009.

[18] K. Leang and S. Devasia, "Feedback-linearized inverse feedforward for creep, hysteresis, and vibration compensation in AFM piezoactuators," *IEEE Trans. Control Syst. Technol.*, vol. 15, no. 5, pp. 927-935, Sep. 2007.

[19] J. Macki, P. Nistri, and P. Zecca, "Mathematical models for hysteresis," *SIAM Rev.*, vol. 35, no. 1, pp. 94-123, 1993.

[20] A. Visintin, "Mathematical models of hysteresis," *The Science of Hysteresis*, G.Bertotti and I.Mayergoyz, Eds. London, U.K.: Academic, pp. 1-123, 2006.

[21] H. Adriaens, W. Koning, and R. Banning, "Modeling piezoelectric actuators," *IEEE/ASME Trans. Mechatron.*, vol. 5, no. 4, pp. 331-341, Dec. 2000.

[22] J. Cruz-Hernandez and V. Hayward, "Phase control approach to hysteresis reduction," *IEEE Trans. Control Syst. Technol.*, vol. 9, no. 1, pp. 17-26, Jan. 2001.

[23] F. Goforth and Z. Gao, "An active disturbance rejection control solution for hysteresis compensation," in *Proc. Amer. Control Conf.*, 2008, pp. 2202-2208.

[24] K. Leang, Q. Zou, and S. Devasia, "Feedforward control of piezoactuators in atomic force microscope systems," *IEEE Control Syst. Mag.*, vol. 29, no. 1, pp. 70-82, Feb. 2009.

[25] M. Goldfarb and N. Celanovic, "A lumped parameter electromechanical model for describing the nonlinear behavior of piezoelectric actuators," *J. Dyna. Syst.,Measure., Control*, vol. 119, pp. 478-485, Sep. 1997.

[26] L. Ljung, *System Identification: Theory for the User*, 2rd ed., Prentice Hall PTR, Upper Saddle River, NJ, 1999.

[27] N. Bajcinca and T. Bunte, "A novel control structure for dynamic inversion and tracking tasks," in *Proc. 16th IFAC World Congress*, 2005.

[28] J. Doyle, B. Francis, and A. Tannenbaum, *Feedback Control Theory*, Macmillan Publishing Co., 1990.

[29] Y. Choi, K. Yang, W. Chung, H. Kim, and I. Suh, "On the robustness and performance of disturbance observers for second-order systems," *IEEE Trans. Automat. Contr.*, vol. 48, no. 2, pp. 315-320, Feb. 2003.